Arabian Journal of Chemistry (2018) xxx, xxx–xxx

King Saud University

Arabian Journal of Chemistry

www.ksu.edu.sa
www.sciencedirect.com

ORIGINAL ARTICLE

Enhanced performance of $BiFeO_3$@nitrogen doped TiO_2 core-shell structured nanocomposites: Synergistic effect towards solar cell amplification

Mohamed Mokhtar Mohamed *, **S.M. Reda**, **Ahmed A. Amer**

Benha University, Faculty of Science, Chemistry Department, Benha 13511, Egypt

Received 27 March 2018; accepted 22 June 2018

KEYWORDS

BFO/n-TiO_2;
Core-shell structure;
DSSC;
Charge transfer;
Heterojunction p-n;
Surface defects

Abstract A core-shell nano-heterostructured perovskite $BiFO_3$@nitrogen doped mesoporous TiO_2 (BFO/n-TiO_2) hydrothermally assembled via using citric acid and polyethlene glycol (PEG) was characterized through XRD, TEM, FTIR, UV–Vis diffuse reflectance, IPCE, N_2 adsorption and impedance spectroscopy. It has been demonstrated that the photovoltaic yield of the 90%N-TiO_2-10%BFO electrode achieves a power conversion efficiency (PCE) of 4.5%, which is 1.85, 2.5, 3 and 1202 times higher than those of 10%N-TiO_2-90%BFO, 50%N-TiO_2-50%BFO, n-TiO_2 and pristine BFO, respectively. It is acknowledged that the former electrode exhibits a significant visible light harvesting capability, lowest band gap (E_g = 2.0 eV) as well as the highest IPCE% (36% at 460 nm) values. The EIS and capacitance results illustrated that 90%N-TiO_2-10%BFO owns excessive charge carriers ($e^- - h^+$); compared to rest of nanocomposites, with a great sparation, to assist boosting the PCE value. This was highly aided by the surface defects seen on the core represented by BFO, which worked as a rational carrier trapper between the N719 dye and the n-TiO_2 shell structure. The surface texturing properties of the nanocomposite forming the 90%N-TiO_2-10%BFO electrode including S_{BET} (Asahi et al., 2001) and pore volume (0.48 $cm^3\ g^{-1}$) have shared significantly in improving the conversion efficiency of such p-n heterojunction based solar cells; which never achieved as such in all BFO-based solar cell devices, with acceptable tunability.

1. Introduction

Electrochemical energy storage and conversion systems including fuel cells, batteries, dye sensitized solar cell (DSSC) as well as electrochemical capacitors (ECs) have attracted lately lots of attention as new ways for green sustainable energies. DSSC is an ongoing technology that accustomed to produce electricity in a wide range of exposed light. However, many problems face DSSC to produce considerable efficiency such as limited

* Corresponding author.
E-mail address: mohamedmokhtar@fsc.bu.edu.eg (M.M. Mohamed).
Peer review under responsibility of King Saud University.

Production and hosting by Elsevier

https://doi.org/10.1016/j.arabjc.2018.06.013
1878-5352

Please cite this article in press as: Mohamed, M.M. et al., Enhanced performance of $BiFeO_3$@nitrogen doped TiO_2 core-shell structured nanocomposites: Synergistic effect towards solar cell amplification3@nitrogen doped TiO_2 core-shell –>. Arabian Journal of Chemistry (2018), https://doi.org/10.1016/j.arabjc.2018.06.013

dye absorption of the incident light (1%), back donation on most used metal oxides, fast recombination of $e^- - h^+$, decreasing surface area of most oxides, and increasing particles size. Accordingly, since most of the problems are concerned with the working electrode (anode), we intended to fabricate an anode electrode capable of transporting electrons more freely with high light harvesting capability without suffering permanent chemical transformation. Among various oxide semiconductor photocatalysts, titanium dioxide has become the most widely used due to its strong oxidizing power, non-toxicity and long-term photostability (Asahi et al., 2001). However, the photocatalytic efficacy of TiO_2 to operate in DSSC is usually limited due to the high recombination rate of photo-induced electrons (e-) and holes (h^+) and to its limited sensitivity to operate only under ultraviolet (UV) light ($\lambda < 380$ nm). Accordingly, the fabrication of nitrogen-doped TiO_2 (n-TiO_2) of a localized N2p above the valence band (V_B) is expected to exhibit band gap narrowing to endow with an appreciable visible light absorptivity (Nakano et al., 2005; Wang et al., 2003). The defect states originated from oxygen vacancies and reduced Ti species (Ti^{3+}) together with n-derived states are shown to contribute to the light absorption characteristics of n–TiO_2 into the visible light region (Li et al., 2009). Hence, to prevent the recombination of charge carriers and to extend the light absorption into visible light region, a constructive conductive substrate is urgently required for enhancing the photocatalytic activity. Amongst oxide photocatalysts, $BiFeO_3$ have attracted much interest because of their attractive electronic structure, lower band gap and light harvesting capabilities (Wu et al., 2016; Qi et al., 2002).

However, decreasing surface areas and fast electron-hole recombination limit their photocatalytic actions together with the huge volume change BFO can browse (Yanko, 1993). Accordingly, the combination of n-TiO_2 with bismuth ferrite (BFO) is expected to develop high solar light absorptivity based on BFO characterization that showed high potentiality in photovoltaic (PV) and ferroelectric applications beside generating efficient charge separation and transport (Taretto and Rau, 2004; Tena-Zaera et al., 2005). In addition, coupling of BFO with the wide band-gap semiconductor TiO_2 is functioned for organic dyes degradation; however, they did not mention nor utilize such a system for photovoltaic applications (Choi et al., 2009). Wu et al. (2010) have investigated the diode-like behaviour of the BFO/ZnO system, without performing any photovoltaic applications. G. G. Khan, et al. (Sarkar et al., 2015), on the other hand, have reported the synthesis of TiO_2 nanotubes for anchoring $BiFeO_3$ (BFO) nanoparticles for their pseudocapacitive properties. They exhibit a specific capacitance of 440 F g^{-1} with ~80% capacity retention at a current density of 2.5 A g^{-1}. It has been shown that Bi deficiency provides hole carriers in $BiFeO_3$ and thus acts as a p-type semiconductor. Oxygen nonstoichiometry in $BiFeO_3$ affects also the diffusion and forms with n-TiO_2 a p-n junction interface able to modulate the delaying of the $e^- - h^+$ recombination process. Despite the moderately related work concerning $BiFeO_3$ in literatures, none have been published regarding the use of BFO as a thin-absorber or a sensitizer for photovoltaic applications to trap solar energy. This was mainly because of the previous shortages alongside some of the parameters need to be tuned such as electron affinity and work-function of different hole-conductor for better obtaining high efficiency. Accordingly, combining BFO with n-TiO_2 of magnificent textural, optical and electronic properties (Wang et al., 2015) will indeed affect the sensitivity of the former for better DSSC efficiency. Accordingly, the strategy mentioned previously concerning the employ of BFO to form a composite with n-TiO_2 is expected to improve the electrochemical performance towards DSSC via inducing a greater separation between e^-/h^+ pairs, permitting more of the reactive species on the catalyst surface, increasing electron transfer as well as enhancing the visible light absorptivity. For the first time, we are going to demonstrate that the nanoferrites $BiFeO_3$/n-TiO_2 heterostructures is a promising bi-functional material as a photovoltaic sensitizer in DSSC devices. Synthesizing nanoferrites BFO/n-TiO_2 photocatalysts via facile hydrothermal methods using the polyethylene glycol template for its advantageous in controlling the particle size, morphology and the degree of aggregation is conducted. The composite materials are characterized by X-ray diffraction (XRD), transmission electron microscopy (TEM), UV–Vis diffused reflectance spectroscopy, impedance spectroscopy (EIS), Fourier-transform Infrared spectroscopy, N_2 adsorption and IPCE. The dc conductivity, σ_{dc}, of as-synthesized materials determined at 25 °C was calculated using the equation $\sigma_{dc} = (l/As)(1/R_{dc})$ where R_{dc} is the sample resistance, l is the sample length, and As is the cross-sectional area. The results are collected employing a programmable automatic LCR bridge (HIOKI 3532-50) and an electrometer (model 6517, Keithley), voltameter (Keithley, 2182), and 5 kV dc power supply.

2. Experimental

2.1. Preparation of BFO

The fabrication of $BiFeO_3$ (BFO) using sol-gel chemistry was adopted using equimolar proportions of $Bi(NO_3)_3{\cdot}5H_2O$ and $Fe(NO_3)_3{\cdot}9H_2O$ to give a total of 0.2 M, followed by agitation for 10 min. At the same time, 20 ml of dilute HNO_3 (20%) solution was added while stirring for attaining a homogenous mixture. Subsequently, 12 g of citric acid was added to the solution followed by the addition of 2 g of PEG as a dispersant agent. The resultant yellowish solution was heated with continuous stirring for 1 h at 80 °C. Subsequently, the concentrated solution mixture was slowly heated up in an oven at 150 °C for 5 h to obtain the powdered material, which annealed at 600 °C for 5 h. The succeeding reactions explain the manufacture of the BFO-sol via hydrolysis and condensation steps (Wang et al., 2013):

$$Bi(NO_3)_3 + Fe(NO_3)_3 + H_2O \rightarrow (NO_3)_{(3-x)}Bi\text{-}(OH)_x + (HO)_x\text{-}Fe\text{-}(NO_3)_{(3-x)} + xNO_2^- + xH^+ \quad (NO_3)_{(3-x)}Bi\text{-}(OH)_x + (HO)_x\text{-}Fe\text{-}(NO_3)_{(3-x)} \rightarrow (NO_3)_{(3-x)}Bi\text{-}O\text{-}Fe(NO_3)_{(3-x)}\cdots + xH_2O$$

2.2. Preparation of nitrogen doped-TiO_2

The synthesis of n-TiO_2 is produced as follows (Mohamed et al., 2017): 1.5 ml titanium (IV) isopropoxide (TIP) dispersed in 3 ml conc. HCl; labeled as solution A, was stirred vigorously till the pale yellow color is formed. The 190 μL of the non-ionic surfactant Brij-35 [$C_{12}H_{25}(OCH_2CH_2)_nOH$]; at 30% W/V + 2 ml distilled water, with 0.02 gm of urea were added to 35 ml methanol in a 250 ml beaker, and labeled as solution B.

Please cite this article in press as: Mohamed, M.M. et al., Enhanced performance of $BiFeO_3$@nitrogen doped TiO_2 core-shell structured nanocomposites: Synergistic effect towards solar cell amplification3@nitrogen doped TiO_2 core-shell –>. Arabian Journal of Chemistry (2018), https://doi.org/10.1016/j.arabjc.2018.06.013

Solution B was added drop by drop to solution A while moderate stirring. An aqueous ammonia solution (30%) was then dropped wisely till pH 7.5. The mixture was stirred for 1 h then poured to a petri dish and kept static at 40 °C for 24 h. The temperature was raised to 50 °C then to 60 °C for 24 h after that it kept at 100 °C for 4 h to ensure accomplishment of the condensation process. The solid product was then grinded in the mortar with a pestle then calcined in air at 400 °C for 2 h with a heating rate of 2 °C/min.

2.3. Preparation of n-TiO_2 doped BFO

An adequate amount of the yellowish BFO sol containg citric acid and PEG surfactant; used to prepare different wt.% of BFO, is added drop-wisely onto the suspension of n-TiO_2 whilst stirring for 1 h. This mixture will then hydrothermally heated at 80 °C for 14 h and finally heated at 600 °C for 5 h. The synthesized composites with different weight ratios were denoted as 10%N-TiO_2-90%BFO, 50%N-TiO_2-50%BFO and 90%N-TiO_2-10%BFO.

2.4. Characterization techniques

X-ray diffractions (XRD) are measured at room temperature using a Philips diffractometer (type PW-3710); equipped with Ni-filtered copper radiation (λ = 1.5404 Å), at 30 kV and 10 mA with a scanning speed of 2θ = 2.5°/min. The Fourier transform infrared (FT-IR) spectra are recorded via a single beam Perkin Elmer Spectrometer (RXI FT-IR), with a resolution of 2 cm^{-1} using the KBr (1:100) method, in the region 4000–400 cm^{-1}. The surface properties namely BET surface area, total pore volume (V_p) and mean pore radius (r) are determined from N_2 adsorption isotherms measured at 77 K using digisorp technique and the samples are out-gassed at 473 K for 3 h at a pressure of 10^{-5} Torr, before starting the measurement. Diffuse Reflectance Ultraviolet–visible spectroscopy (UV–vis DRS) of the samples are carried out at room temperature using UV–vis JASCO spectrophotometer, V-570, in the range of 200–1000 nm. The edge energies (E_g) of allowed transitions are determined by finding the intercept of the straight line in the low-energy rise of the plot of $\alpha h\upsilon = A(h\upsilon - Eg)^{n/2}$. TEM micrographs are measured using a FEI; model Tecnai G20, Super twin, double tilt 1010, at an accelerating voltage of 200 KV. Electrochemical impedance spectroscopy (EIS) measurements were performed using an EG&G PAR galvanostat/potentiostat, model type 273. The justification of the impedance spectra was determined based on the Kramers-Kronig transformation. The EIS electrodes were made via mixing PVF with carbon black together with our synthesized material with ratios of 5:10:85, respectively. This paste was deposited onto the FTO conducting glass. The electrodes were transferred to an electrochemical cell containing 0.5 M H_2SO_4 solution and attached with a thin platinum electrode and a reference electrode composed of $Hg/HgSO_4$. The EIS measurements were performed in the frequency range from 10 μA to 100 mA, frequency margin of 0.1 Hz–140 kHz and at constant potential equal 10 mV.

2.5. Photovoltaic efficiency measurements

The photoelectrochemical solar cell was synthesized using a viscous paste of the manufactured catalysts. It was prepared by adding 1 ml of triton X-100 to 0.05 g of each catalyst. The colloidal solution was put on the conducting glass F-doped SnO_2 layer (Pilkington Kappa Energy Float), of sheet resistance ~19–22 V cm. The colloidal film was fired at 673 K for 1 h. The sintered colloidal x$BiFO_3$/n-TiO_2 films were coated with N719 dye of 2.73×10^{-4} mol/l conc. ethanol by dipping the film for ca. 36 h to obtain electrodes with 15 mm thickness. The counter electrode consisted of the same conducting glass coated with graphite film was also made. The counter electrode was placed directly on the top of the dye coated x$BiFO_3$/n-TiO_2 films, permitting the two ends of the glass for application of an electrical contact. The electrolyte containing 0.3 M KI-0.03 M I_2 dissolved in acetonitrile was forced up via the capillary force into the inter electrode space. The I–V characteristic for the cell was examined in the presence of light using an ELH-lamp at a light intensity of 100 mW/cm^2. The voltage and current were recorded using Keithly voltammeter 175A and Keithly electrometer 614, respectively. The fill factor was calculated using the following relation: $FF = V_m\ I_m/V_{OC}\ I_{SC}$, where V_m and I_m are respectively, voltage and current for maximum power output. The solar cell efficiency is calculated (η_y) using the following relation: $\eta_y = V_{oc}\ I_{sc}\ FF/P_{in}$ where P_{in} is the power of the incident light. Monochromatic incident photon conversion efficiency (IPCE) spectra were measured using a home-made lock-in-based setup equipped with a calibrated Si/Ge photodiode, as reference detector. The light from the halogen and Xenon lamps was spectrally dispersed using a monochromator with a set of gratings to cover the wavelength range from 300 to 900 nm. The obtained current densities were converted into incident photon-to-current conversion efficiencies (*IPCE*) by using equation: $IPCE = ((1240/\lambda) * (I/P_{in})) * 100$ where $P_{in} = 30\,W$.

3. Results and discussion

3.1. XRD and morphology characteristics

Fig. 1 displays the XRD patterns of n-TiO_2, bismuth ferrite (BFO), 10%n-TiO_2-90%BFO, 50%n-TiO_2-50%BFO and 90%n-TiO_2-10%BFO catalysts synthesized hydrothermally

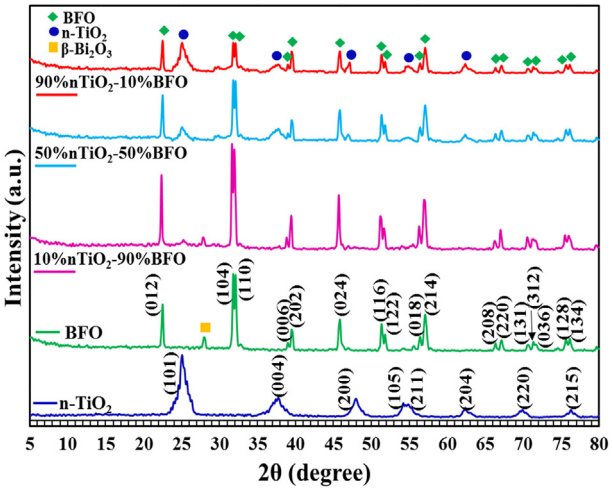

Fig. 1 XRD patterns of n-TiO_2, BFO, 10%n-TiO_2-90%BFO, 50%n-TiO_2-50%BFO and 90%n-TiO_2-10%BFO.

and calcined at 600 °C. It is shown that all the reflection peaks in the pattern of BFO are well crystallized and indexed to the perovskite structure of $BiFeO_3$ (JCPDS card No. 86-1518) with a residual peak at $2\theta = 28.2°$ for β-Bi_2O_3 assigned to the (3 1 0) plane. The peak splitting shown in the BFO pattern indicative of the rhombohedral structure is consistent with the BFO ceramics work depicted previously (Zhang et al., 2005). The XRD pattern of n-TiO_2 indicates peaks at 25.2°, 37.8°, 48.0°, doublet at 54°and 55.0°, 62.6°, 70.3° and 76.2, those indexed respectively to the (1 0 1), (0 0 4), (2 0 0), (1 0 5), (2 1 1), (2 0 4), (2 2 0) and (2 1 5) planes of anatase TiO_2 (JCPDS Card 21-1272). The spectrum of 10%n-TiO_2-90%BFO reveals the hybridization of both of the components forming the latter material via exposing (1 0 1) and (0 0 4) reflections of n-TiO_2 together with all the intensified reflections mentioned for the BFO. No Bargg peaks shift are depicted for the 10%n-TiO_2-90%BFO pattern and the crystallite size is increased compared with that of the pristine BFO. This suggests the absence of any lattice strain change, possibly due to the similarity of the ionic radii of both of the host (Fe^{3+}) and guest (Ti^{4+}) cations. Intensification of BFO crystallites size reflects ordering of the local structural and the increase in the nucleation rate. Increasing the loading of n-TiO_2 into 50% and 90% over those of BFO causes the retain of TiO_2 peaks intensities with vanishing the peak of β-Bi_2O_3 (3 1 0), while developing another one due to the α-Bi_2O_3 (2 0 0) phase.

Fig. 2a for n-TiO_2 shows polyhedral structure composed mainly of hexagonal and rhombus shapes with an average diameter equal ~20 nm. The TEM image of the bismuth ferrite Fig. 2b) exhibits spherical like sheets with an average diameter equal 10 nm and of a notable agglomeration based on the appreciable magnetic properties of BFO used to have (Loh et al., 2014). In the image of 90%n-TiO_2-10%$BiFO_3$ Fig. 2c), a core-shell de-agglomerated uniform spherical nanoparticles of an average diameter of 10 nm was appeared. Indeed, coating BFO with n-TiO_2 assists the attainment of discrete nanoparticles and prevents coalescing of the former via the exhibited strong interaction with the n-TiO_2. This is ascertained via changing the morphology from polyhedral (n-TiO_2)-nanoparticles (BFO) into spherical nanoarchitecutre upon forming the nanocomposite with keeping the particle size unaffected for BFO and BFO/n-TiO_2 samples. The SAED pattern (inset) indicates that n-TiO_2 decorates BFO via emergence of (1 0 1), (0 0 4) and (2 0 0) crystal facets of the former on (0 1 2) of the latter. This emphasizes the intimate interaction between n-TiO_2 and BFO and rather their arrangement in which the former is considered as a shell for the bulk BFO. Apparently, the shell of the nanoparticles; which displays some

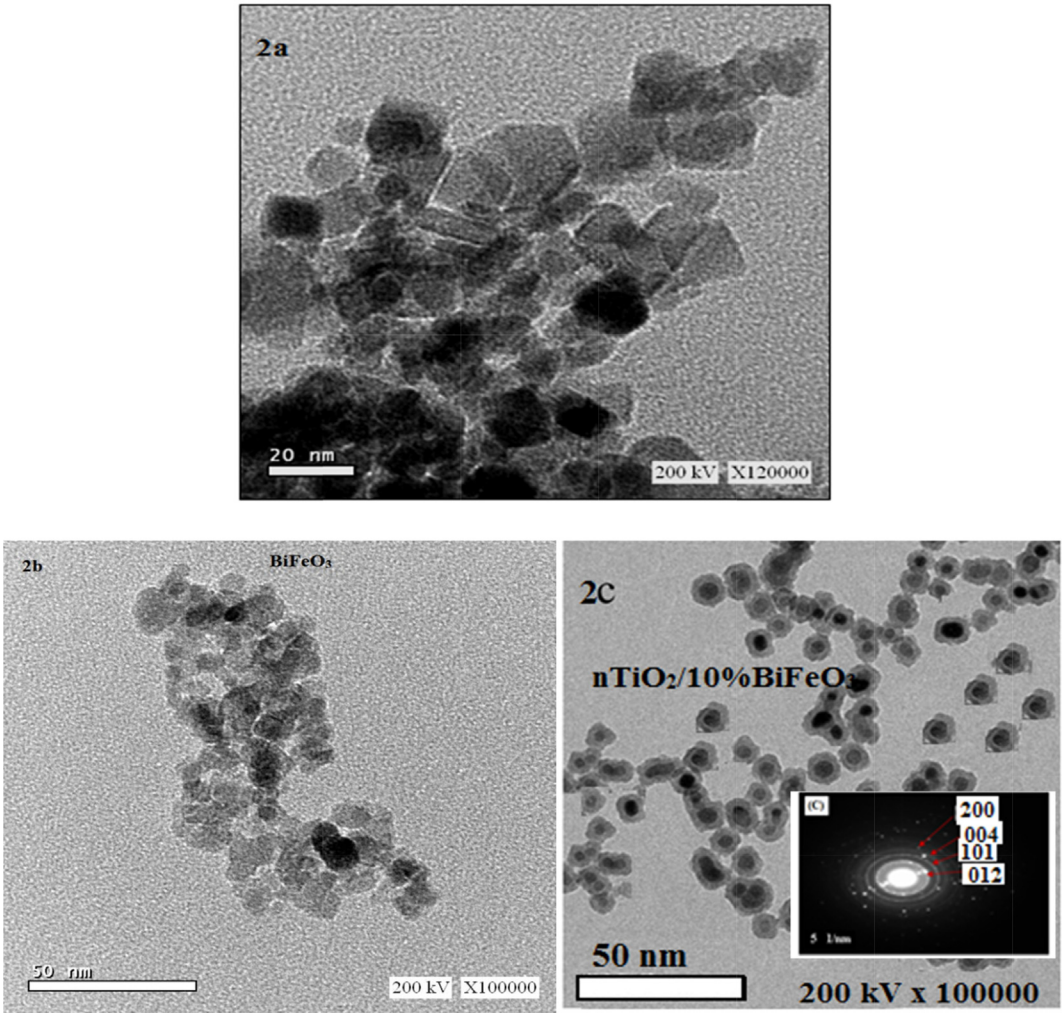

Fig. 2 TEM images of n-TiO_2, BFO, and 90%n-TiO_2-10%BFO.

Please cite this article in press as: Mohamed, M.M. et al., Enhanced performance of $BiFeO_3$@nitrogen doped TiO_2 core-shell structured nanocomposites: Synergistic effect towards solar cell amplification3@nitrogen doped TiO_2 core-shell –>. Arabian Journal of Chemistry (2018), https://doi.org/10.1016/j.arabjc.2018.06.013

defects, demonstrates lesser crystallinity relative to the core of an average diameter of 5 nm. It seems that the use of PEG and citric acid helps the promotion of the core-shell structure with such stability that never achieved before, likely via forming citrate BFO-compound and PEG carbonizatioin following the annealing step.

3.1.1. Vibrational, optical and IPCE characteristics

The FTIR spectra of pristine n-TiO_2, BFO and n-TiO_2-BFO nanocomposites are shown in Fig. 3. Evidently, pure BFO has shown a band at 1630 cm^{-1} due to water bending vibrations in addition to two broad bands at 561 and 438 cm^{-1} attributed respectively, to the Fe—O stretching and O—Fe—O bending vibrations. The latter bands characterize the octahedral FeO_6 groups in perovskite compounds. The FTIR spectrum of n-TiO_2 indicates a peak at 1630 cm^{-1} due to the bending vibrations of either O—H or N—H beside, another one at 1363 cm^{-1} correlated to the C—O bonds vibrations (Peng et al., 2017) and confirms the presence of the Birj surfactant residuals. The exhibited saturation seen in the margin from 450 to 900 cm^{-1} corresponds to the vibrational mode of Ti—O—Ti in anatase structure; as XRD confirmed. The spectrum of 10%n-TiO_2-90%BFO indicates two bands as those shown for BFO (Asahi et al., 2001) but with more sharpness and shift in wavenumbers into respectively 444 cm^{-1} and 545 cm^{-1}. This could give a hint about the involvement of the Ti^{4+} ions (0.74 Å) into the BFO structure and most probably replacing the Fe^{3+} ion (0.78 Å), causing insignificant change in the interplanar distance, as XRD supported. The absence of any impurity peaks in the XRD of this sample except that of β-Bi_2O_3 existed in n-TiO_2 highlights that n-TiO_2 reacts with BFO but rather emphasizes the substitution of Ti^{4+} at the Fe^{3+} sites more willingly than that at Bi^{3+} sites, of higher ionic radius (1.17 Å). Further increase of n-TiO_2 weight percentages into 50% and 90% causes a marked decrease in intensity of 444 cm^{-1} and 545 cm^{-1} bands to confirm the latter assignment concerning the substitution process. Additionally, shifting the bands at 1363 and 1630 cm^{-1} seen in n-TiO_2 into 1393 and 1635 cm^{-1} in 50%n-TiO_2-50%BFO and 90%n-TiO_2-10%BFO samples was depicted. This indeed gives a hint about the strong interaction between BFO and n-TiO_2

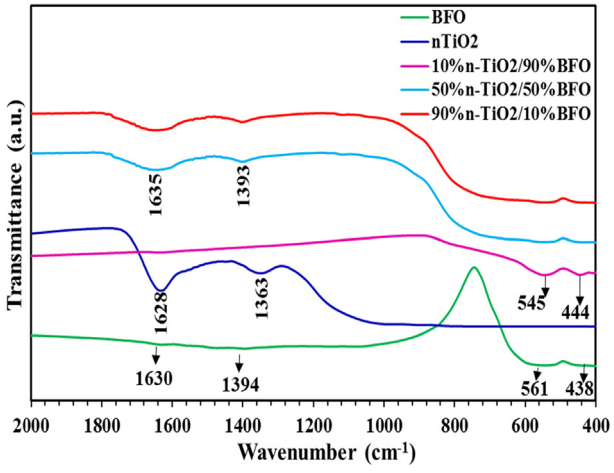

Fig. 3 FTIR spectra of n-TiO_2, BFO, 10%n-TiO_2-90%BFO, 50%n-TiO_2-50%BFO and 90%n-TiO_2-10%BFO.

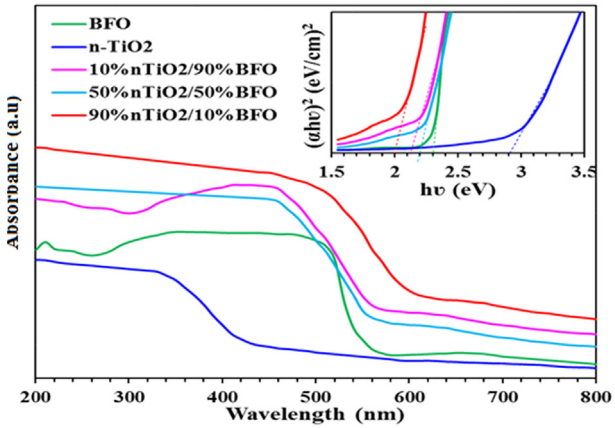

Fig. 4 UV–vis DRS spectra of n-TiO_2, BFO, 10%n-TiO_2-90% BFO, 50%n-TiO_2-50%BFO and 90%n-TiO_2-10%BFO. Inset is the corresponding plots of $(\alpha h\upsilon)^2$ vs. hυ for E_g determination.

moieties, at such high loadings of the latter. Additionally, the decrease in intensity of the latter bands compared to the corresponding analogue in n-TiO_2 gives an idea about the move of BFO into substitutional sites in n-TiO_2, with keeping the BFO structure intact.

The UV–Vis DRS of the n-TiO_2 and BFO samples together with their different composites are shown in Fig. 4. The spectrum of n-TiO_2 exhibits an absorption edge at 450 nm whereas that of BFO displays an edge at 550 nm, with a noticeable increase in absorbance throughout all-region exceeding that of the pristine n–TiO_2. The 10%n-TiO_2-90%BFO spectrum presents an absorption edge at 600 nm and light absorption surpassing the individual n-TiO_2 and BFO samples. Increasing the n-TiO_2 percentage into 50% in 50%n-TiO_2-50%BFO causes insignificant improve in absorbance towards the red region to have an edge at 590 nm, lower than that of 10%n-TiO_2-90%BFO. However, the spectrum of 90%n-TiO_2-10%BFO has shown an outstanding absorption edge shift into 660 nm with a distinctive increase in the light absorption throughout the whole margin. Although all materials show absorption in visible light with different degrees, the 90%n-TiO_2-10%BFO catalyst was the best. The band gap energies were determined using the typical equation: $\alpha h\upsilon = A(h\upsilon - Eg)^{n/2}$ where α, h, n, E_g and A are respectively correlated to absorption coefficient, Planck's constant, frequency of light, band gap energy, and a constant. The obtained corresponding plots seen in the inset in Fig. 4 indicate E_g values of 3, 2.3, 2.18, 2.2 and 2.0 eV for n-TiO_2, BFO, 10%n-TiO_2-90%BFO, 50%n-TiO_2-50%BFO and 90%n-TiO_2-10%BFO, respectively. Undoubtedly, the calculated E_g values were in concordance with the edges values seen in the UV–Vis results for the different samples, comprehending that the 90%n-TiO_2-10%BFO sample owns the narrowest band gap value and the highest capability for the visible light absorption. Apparently, BFO induces stronger visible optical absoption while n-doped TiO_2 induces more significant band gap narrowing to cope into synergistic effect between them. The synergism is virtually affected by the electronic modification that produced from the N 2p states near valence band of TiO_2 and the middle states in the band gap associated with the doped BFO.

Please cite this article in press as: Mohamed, M.M. et al., Enhanced performance of $BiFeO_3$@nitrogen doped TiO_2 core-shell structured nanocomposites: Synergistic effect towards solar cell amplification3@nitrogen doped TiO_2 core-shell –>. Arabian Journal of Chemistry (2018), https://doi.org/10.1016/j.arabjc.2018.06.013

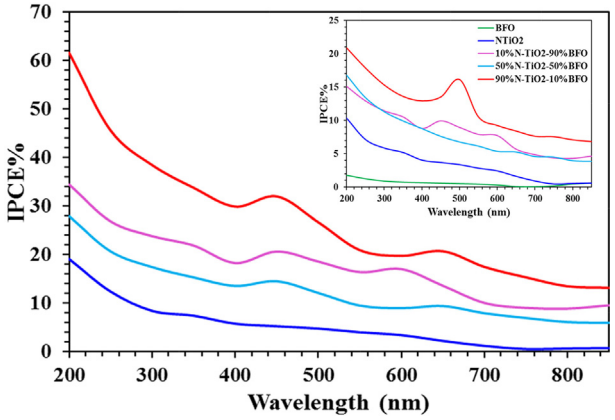

Fig. 5 IPCE curves of N719 sensitized n-TiO_2, BFO, 10%n-TiO_2-90%BFO, 50%n-TiO_2-50%BFO and 90%n-TiO_2-10%BFO electrodes. Inset is typical spectra without dye.

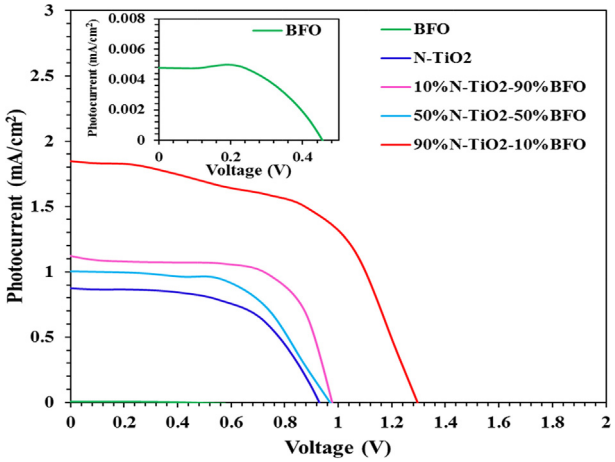

Fig. 6 Photovoltaic I-V curves for n-TiO_2, BFO (inset), 10%n-TiO_2-90%BFO, 50%n-TiO_2-50%BFO and 90%n-TiO_2-10%BFO electrodes in DSSCs.

The incident-photon to current conversion efficiency plots with dye or free of dye (inset Fig. 5) determined to scan its variation with the wavelength for all nanocomposites were shown in Fig. 5. Obviously, IPCE percent values diminish with increasing the wavelength from 200 to 850 nm. Compatible with the UV–Vis results, the 90%n-TiO_2-10%BFO electrode shows the maximum IPCE; in the visible range, at 500 nm that amounts 18% (inset Fig.). Another hump of a maximum at 760 nm of IPCE equal 9% was also depicted. The electrode IPCE values exceeded those of 50%n-TiO_2-50%BFO and 10%n-TiO_2-90%BFO ones, which showed IPCE values of 10% and 8%, respectively at closer wavelengths to the 90% n-TiO_2-10%BFO electrode. Unlike the UV–Vis results, the IPCE of n-TiO_2 shows higher values than that of BFO revealing the efficacy of the former to convert light into electrical energy than the latter. This indeed raises the difficulty of transferring light into current while using the BFO electrode although of the appreciable amount of light absorbed by this sample. On the other hand, n-TiO_2 possesses higher number of charge carriers when illuminated by light, revolving higher electrical current density. Comparing the N719 IPCE synthesized spectra with those without dye, a stronger absorption was observed in the range of 400–700 nm especially for 90% N-TiO_2-10%BFO and 10%N-TiO_2-90%BFO composites and almost double those without dye (inset). The IPCE of the 90%N-TiO_2-10%BFO cell indicates better absorption across a broad spectral range. These results inform that the N719 sensitized 90%N-TiO_2-10%BFO absorbs more solar energy and causes shift of the peak at 500 nm to 460 nm, upon dye sensitization with revealing another one at 650 nm. The former shift confirms the strong interaction between the dye/nanocomposite where the second peak verifies capturing of the longer wavelength light by the N719—nanocomoposite, covering wide ranges in the visible light. Enhancing the IPCE spectral area of nanocomposites compared to the individual analogue highlights the importance of n-TiO_2/BFO hybridization at specific ratios as evolved for the 90%n-TiO_2-10%BFO catalyst.

3.2. Solar cell efficiency

A PCE as high as 4.5% was achieved for 90%n-TiO_2-10% BFO exceeding the rest of the electrodes as illustrated in the J–V curves, seen in Fig. 6. The resulting photovoltaic parameters are determined and presented in Table 1. The latter electrode was distinguished by a J_{SC} of 1.85 mA cm^{-2}, an open-circuit voltage (V_{OC}) of 1.3 V and a fall factor (FF) of 0.55, while the n-TiO_2 photoanode of the same thickness gave a PCE of only 1.5%, a J_{SC} of 0.9 mA cm^{-2} and V_{OC} of 0.92 V, surpassing those of the BFO electrode (0.037%, 0.0048 mA cm^{-2}, and 0.46 V). Apparently, the synergic effect between n-TiO_2 and BFO (in-set Fig.) increases the efficiency of the composites due to the perceived boosting in J_{SC}, which probably correlated to increasing the adsorption of the dye amount. Consistently, the Voc of the 90%n-TiO_2-10%BFO device was larger (1.3 mV) than the other nanocomposites (0.99 mV), signifying better separation of photoexcited $e^- - h^+$ pair and rather proposes an interface between the components forming the electrode facilitating charges tranfer. This also confirms minimization of the photogenerated electron back transfer at the electrode/electrolyte interface; as will be confirmed latter by the EIS analysis.

The increase in J_{SC} was in the order; 90%n-TiO_2-10%BFO > 10%n-TiO_2-90%BFO > 50%n-TiO_2-50%BFO. In concordance, the surface area and the pore volume values contributed much to the dye adsorption process via enhancing the S_{BET} into 246 m^2 g^{-1} and pore volume (V_p) into 0.48 cm^3 g^{-1} for 90%n-TiO_2-10%BFO exceeding those of 50%n-TiO_2-50% BFO (201 m^2 g^{-1}, 0.41 cm^3 g^{-1}) and 10%n-TiO_2-90%BFO (195 m^2 g^{-1}, 0.21 cm^3 g^{-1}). Whereas, n-TiO_2 showed S_{BET} of 157 m^2 g^{-1} and V_p of 0.43 cm^3 g^{-1}. In spite of the marked increase in the S_{BET} of the former, it also generates the deepest volume; susceptible for improving the dye adsorption, rather than the other correspondent catalysts. This explores the strong enforcement of the BFO; at the 10% ratio, deep inside the n-TiO_2 mesopores (54.7 Å). These results were in agreement with the optical and IPCE outcomes through which, the 90%n-TiO_2-10%BFO catalyst employed the best light absorption during the 200–800 nm region alongside exhibiting the narrowest band gap (Eg = 2.0 eV) and the highest IPCE values (36% at 450 nm). It seems also that the light scattering affect much the J_{SC} values as elucidated in the IPCE spectra that showed a general diminish as a function of wavelength

Please cite this article in press as: Mohamed, M.M. et al., Enhanced performance of $BiFeO_3$@nitrogen doped TiO_2 core-shell structured nanocomposites: Synergistic effect towards solar cell amplification3@nitrogen doped TiO_2 core-shell –>. Arabian Journal of Chemistry (2018), https://doi.org/10.1016/j.arabjc.2018.06.013

Table 1 The performance of n-TiO_2 and BFO/n-TiO_2 electrodes in solar cells with N719.

Sample	I_{sc} (mA)	V_{oc} (V)	P_{max}	*FF*	*%Eff.*
BFO	0.0048	0.46	1.1×10^{-3}	0.5	3.7×10^{-3}
N-TiO_2	0.9	0.92	0.45	0.543	1.5
10%N-TiO_2-90%BFO	1.1	0.99	0.722	0.663	2.41
50%N-TiO_2-50%BFO	1	0.99	0.533	0.538	1.78
90%N-TiO_2-10%BFO	1.85	1.3	1.32	0.55	4.5

for all the catalysts. In this essence, unexpectedly the 10%n-TiO_2-90%BFO catalyst showed higher visible light absorptivity and incident photon to current conversion than 50%n-TiO_2-50%BFO and thus depicted an efficiency of 2.41% surpassing that of the latter (1.78%) Table 1. This delivers a marked increase in the fill factor value surpassing all devices and to comprehend the best photogenerated electron transfer. However decreasing its efficiency compared to the 90%n-TiO_2-10%BFO device could be due to the mesoporous nature of latter as well as for the sufficient pores accessible in the photoanodic film for better electrolyte functioning, which are responsible for successful regeneration of the sensitizer nanoparticles.

Enhancement of the photovoltaic efficiency of the 90%n-TiO_2-10%BFO electrode (4.5%) was found to exceed some others containing $BiFeO_3$ such as ZnO/BFO (0.38%), Nd^{3+}-doped $BiFeO_3$ polycrystalline ceramics (0.82%), ITO/poly-BFO/Pt (0.125%) and $BiFeO_3$/TiO_2-nanotubes (3.2%), all tested under similar simulated sunlight conditions (100 mW cm^{-2}, AM 1.5G simulated sunlight) (Chen et al., 2011; Zhu et al., 2013; Nagaveni et al., 2004; Moriguchi et al., 1995).

As formerly testified, metals ion incorporation into TiO_2 are going to modify the interfacial charges transfer and hereafter influence the optical absorption (Li et al., 2009; Feng et al., 2015). Expectedly, the red shift noticed in the absorption spectra of nanocomposites is basically due to the diffusion of Fe; and may be Bi, into the TiO_2 phase (Humayun et al., 2016) principally due to the formation of the core-shell structure of $BiFeO_3$@n-TiO_2, as TEM confirmed. Such core-shell structure formed between the two semiconductors ($BiFeO_3$@n-TiO_2) is going to facilitate the electronic interaction at the junction point between them i.e. the accumulated photoelectrons are expected to improve the efficacy of the photocatalytic performance. This indeed will also affect the availability of charge carriers via amplifying their separation rather than their recombination. The assembled heterojunction of BFO@n-TiO_2 (core-shell) and the rising up of the BFO fermi level where descending that of n-TiO_2, of higher negativity, is well admitted (Aroutiounian et al., 2007). Thus, exposure to solar irradiation with exceed photon energy compared to the CB of BFO; of lower CB and E_g than n-TiO_2, will excite electrons from BFO CB to the similar one in n-TiO_2 for well solar energy utilization. Accordingly, the nanocomposite 90%n-TiO_2-10%BFO improved the efficiency by 3 times that of n-TiO_2 and 1202 times for BFO, which suffers very relaxed electrons in the CB bottom and an inadequate charges separation (Aroutiounian et al., 2007), affecting seriously the solar energy consumption. The obtained results form the J–V curves and TEM images testified that increasing the BFO thickness decreases the current (J_{sc}) significantly as compared to the lowest amount (10% BFO). This suggests that the thickness plays a marked role in the electron transfer rate form N719 into the composite of n-TiO_2/BFO. Since 90%n-TiO_2-10%BFO accomplished the highest efficiency, one can admit that the thickness around 5 nm (as TEM elaborated) is quite good to facilitate the electron transfer. Additionally, the surface defects seen on the BFO core structure could regulate the electron transfer from the dye into n-TiO_2 via working as electron trap and to assist in the dye adsorption process.

Accordingly, to understand the charge transfer characteristics of the nanocomposites and especially the separation efficacy between electron/hole pairs and to reveal to what extent it affected by the structure, EIS measurements were examined. The EIS Nyquist plots seen in Fig. 7 displays the impedance spectra of the nanocomposites together with those BFO (inset) and n-TiO_2 materials in H_2SO_4 electrolyte. The impedance parameters values are measured and presented in Table 2. The charge transfer resistance values (R_{CT}) verified at an open circuit potential for the nanocomposites were in the sequence; 50%n-TiO_2-50%BFO (150 Ω) > 10%n-TiO_2-50%BFO (100 Ω) > 90%n-TiO_2-10%BFO (86 Ω). Whereas, those of

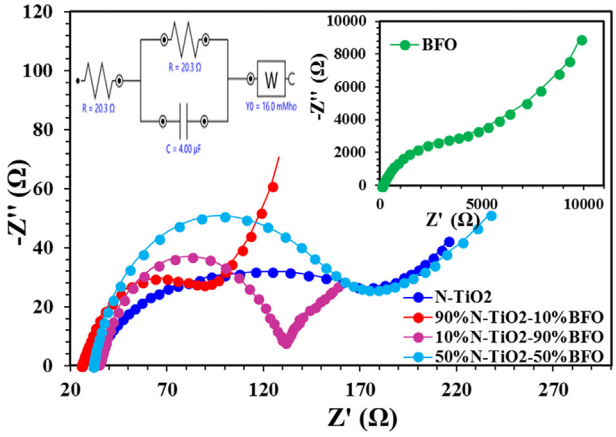

Fig. 7 Nyquist plots of all the samples in H_2SO_4, inset is the 90%n-TiO_2-10%BFO circuit.

Table 2 Different types of resistances for all the samples.

Sample	R_s (Ω)	R_{ct} (Ω)	τ (s)
BFO	34	6.4×10^3	5.4×10^{-2}
N-TiO_2	32	168	1.7×10^{-2}
10%N-TiO_2-90%BFO	35	100	7.0×10^{-4}
50%N-TiO_2-50%BFO	32	150	1.4×10^{-3}
90%N-TiO_2-10%BFO	26	86	8.5×10^{-3}

Please cite this article in press as: Mohamed, M.M. et al., Enhanced performance of $BiFeO_3$@nitrogen doped TiO_2 core-shell structured nanocomposites: Synergistic effect towards solar cell amplification3@nitrogen doped TiO_2 core-shell –>. Arabian Journal of Chemistry (2018), https://doi.org/10.1016/j.arabjc.2018.06.013

n-TiO_2 and BFO employed charge transfer resistance of 168 Ω and 6400 Ω, respectively. The intercept across the Z′ axis at the high frequency closing point assigned to the total series resistance (Rs); which count on different types of resistances such as those electrolyte, intrinsic active material and contact, exhibit comparable values between 32 and 34 Ω with the exception of 90%n-TiO_2-10%BFO that showed a lower value comprised of 26 Ω. It appears that all the samples presented in Fig. 7 produced one semicircle at the high frequency zone and a straight line at the low frequency one, signifying a mixed process of respectively, charge transfer and diffusion. The EI spectra of nanocomposites are not comparable in the sense that larger semicircular radius; characterizing larger electron transport resistance, was seen for 50%n-TiO_2-50%BFO and 10%n-TiO_2-90%BFO electrodes. Whereas, 90%n-TiO_2-10%BFO features lower electron resistance as well as high separation efficiency for the photo-generated e^-/h^+ pairs. Indeed, the imperfection and the oxygen vacancies mediated by the core-shell structure observed in the nanocompoites and found excessively on 90%n-TiO_2-10%BFO; as XRD and TEM confirmed, nullify greatly the recombination between electrons and holes, comparatively. The straight lines seen by the low frequency zone illustrates that the 90%n-TiO_2-10%BFO electrode owns higher potential towards ions diffusion compared to rest of the composites, although it suffers electronic transfer at some frequencies when compared with the pristine n-TiO_2 electrode Fig. 7. Increasing the ions diffusion on the 90%n-TiO_2-10%BFO electrode than rest of the electrodes is explained in view of increasing significantly the pore volume of that composite than the correspondents ones; as N_2 sorptiometry confirmed. The equivalent circuit drawing result of the 90%n-TiO_2-10%BFO electrode was traced in Fig. 7 inset and showed closeness of the circuit with information obtained from EIS, and in particular it shows the predominance of the double layer capacitance. The charge transfer was in parallel with the diffusion impedance (W; Wurburg) and in series with the capacitance and they all in series with the electrolyte and capacitance resistance. Accordingly, the superior electron transfer notified in 90%n-TiO_2-10%BFO of higher S_{BET} is conceivably owing to the distinctive core-shell structure containing mesoporosity type of pores, diminished crystallites size (10 nm) and to the pore volume depth.

Consistently, calculation of the capacitance for all nanocomposite electrodes based on using the following equation was calculated and presented in Table 3, to configure the charges storage capability: $X_C = 1/\omega C = 1/2\pi fC$,Where X_C is the capacitor opposition in ohms (Ω), ω is angular frequency in rad/s = 2πf where f is the frequency in Hz and C is the capacitance in farads. The capacitance values, which dependent not only on the catalyst composition but also on the morphological structure evidenced the highest value for

Table 3 Specific capacitance (C_{sp}) of all the samples performed in 0.5 M H_2SO_4.

Sample	Capacitance (F/cm^2)
BFO	2.5×10^{-5}
N-TiO_2	1.6×10^{-3}
10%N-TiO_2-90%BFO	3.64×10^{-3}
50%N-TiO_2-50%BFO	2.5×10^{-3}
90%N-TiO_2-10%BFO	6×10^{-3}

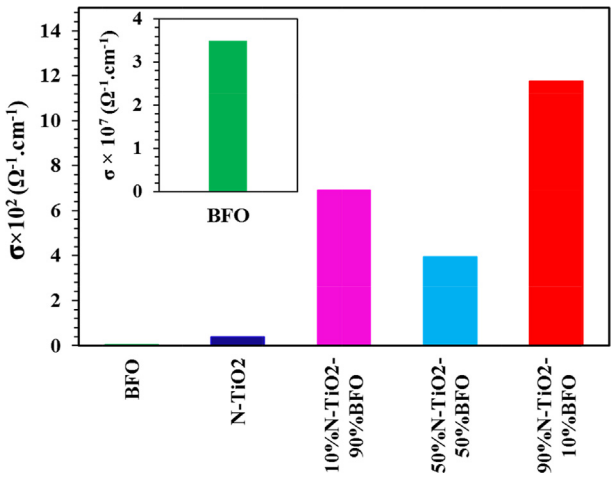

Fig. 8 Electrical conductivity of BFO, N-TiO_2, 10%N-TiO_2-90%BFO, 50%N-TiO_2-50%BFO and 90%N-TiO_2-10%BFO catalysts.

90%n-TiO_2-10%BFO comprised of 0.00364F cm^{-2}, which exceeded that of 10%n-TiO_2-90%BFO by 1.6 times and 50% n-TiO_2-50%BFO by 2.4 times. This highlights the presence of surface problems in the latter two samples obstructing properly the charges transfer process. These examinations concerning impedance and capacitance values clarified the role progressed by 90%n-TiO_2-10%BFO in increasing the charges density as well as their separation efficacy.

The electronic transfer capability of the as-synthesized nanocomposites was tested and presented in Fig. 8, to comprehend the charge carriers ($e^- - h^+$) concentration with the great sparation. Evidently, the 90%n-TiO_2-10%BFO composite shows an excellent electron conduction whereas BFO elucidates the highest resistivity. In this context, the sequence of decreasing the conductivity was in the order; 90%n-TiO_2-10%BFO ($11.7 \times 10^{-2}\,\Omega^{-1}\,cm^{-1}$) > 10%n-$TiO_2$-90%BFO ($6.91 \times 10^{-2}\,\Omega^{-1}\,cm^{-1}$) > 50%n-$TiO_2$-50%BFO ($3.94 \times 10^{-2}\Omega^{-1}\,cm^{-1}$) > n-$TiO_2$ ($3.9 \times 10^{-3}\,\Omega^{-1}\,cm^{-1}$) > BFO ($3.5 \times 10^{-7}\,\Omega^{-1}\,cm^{-1}$). Illustratively, the BFO resistivity is successfully decreased via the decoration with n-TiO_2. It seems that increasing the n-TiO_2 concentration affects the charge carrier concentration and mobility, which are the factors affecting the conductivity. It seems that decreasing the crystallite size of 90%N-TiO_2-10%BFO; as XRD and TEM confirmed, assists electrons transfer via the induced interface formed between BFO and n-TiO_2.

4. Conclusions

The core-shell heterojunction interface of BFO@n-TiO_2 synthesized using citric acid-PEG template; under hydrothermal condition for the first time, has shown photovoltaic efficiency via using DSSC comprised of 4.5% for the 90%n-TiO_2-10% BFO electrode; exceeding so far many of BFO based nanomaterials. The characterization results revealed that the combined light harvesting capability, narrow band gap and surface defects in $BiFeO_3$, which assisted the separation of photogenerated charge carriers, promoted the photovoltaic efficiency. Very well correlations between the thickness of the core BFO, surface texturing properties, morphology and charge

Please cite this article in press as: Mohamed, M.M. et al., Enhanced performance of $BiFeO_3$@nitrogen doped TiO_2 core-shell structured nanocomposites: Synergistic effect towards solar cell amplification3@nitrogen doped TiO_2 core-shell –>. Arabian Journal of Chemistry (2018), https://doi.org/10.1016/j.arabjc.2018.06.013

transfer rate were discussed in the light of their effect on the PCE responses. It is highly recognized that this kind of materials at the mentioned weight ratio might open up a new window for solar cell improvements based on DSSCs.

Acknowledgments

The Authors would like to thank the scientific research box office at Benha University for their support in carrying out this work.

References

Aroutiounian, V.M., Arakelyan, V.M., Shahnazaryan, G.E., Hovhannisyan, H.R., Wang, H., Turner, J.A., 2007. Photoelectrochemistry of tin-doped iron oxide electrodes. Sol. Energy 81, 1369–1376.

Asahi, R., Morikawa, T., Ohwaki, T., Aoki, K., Taga, Y., 2001. Visible-light photocatalysis in nitrogen-doped titanium oxides. Science 293, 269–271.

Chen, B., Li, M., Liu, Y., Zuo, Z., Zhuge, F., Zhan, Q.F., Li, R.W., 2011. Effect of top electrodes on photovoltaic properties of polycrystalline $BiFeO_3$ based thin film capacitors. Nanotechnology 22, 195201.

Choi, T., Lee, S., Choi, Y.J., Kiryukhin, V., Cheong, S.W., 2009. Switchable ferroelectric diode and photovoltaic effect in BiFeO3. Science 324, 63–66; I. Padawer, MS Thesis (adv. Dr. Jason Baxter), Drexel University (Chemical and Biological Engineering), 29 May 2009.

Feng, H.J., Yang, K., Deng, W., Li, M., Wang, M., Duan, B., Guo, X., 2015. The origin of enhanced optical absorption of the $BiFeO_3$/ZnO heterojunction in the visible and terahertz regions. Phys. Chem. Chem. Phys. 17, 26930–26936.

Humayun, M., Zada, A., Li, Z., Xie, M., Zhang, X., Qu, Y., Jing, L., 2016. Enhanced visible-light activities of porous $BiFeO_3$ by coupling with nanocrystalline TiO_2 and mechanism. Appl. Catal. B: Environ. 180, 219–226.

Li, S., Lin, Y.H., Zhang, B.P., Li, J.F., Nan, C.W., 2009. $BiFeO_3/TiO_2$ core-shell structured nanocomposites as visible-active photocatalysts and their optical response mechanism. J. Appl. Phys. 105, 054310.

Li, S., Lin, Y.H., Zhang, B.P., Li, J.F., Nan, C.W., 2009. Photocatalytic and magnetic behaviors observed in nanostructured $BiFeO_3$ particles. J. Appl. Phys. 105, 5.

Loh, L., Briscoe, J., Dunn, S., 2014. Enhanced performance with bismuth ferrite perovskite in ZnO nanorod solid state solar cells. Nanoscale 6, 7072–7078.

Mohamed, M.M., Bayoumy, W.A., Goher, M.E., Abdo, M.H., El-Ashkar, T.M., 2017. Optimization of α-Fe_2O_3@Fe_3O_4 incorporated N-TiO_2 as super effective photocatalysts under visible light irradiation. Appl. Sur. Sci. 412, 668–682.

Moriguchi, I., Maeda, H., Teraoka, Y., Kagawa, S., 1995. Preparation of TiO_2 ultrathin film by newly developed two-dimensional sol-gel process. J. Am. Chem. Soc. 117, 1139–1140.

Nagaveni, K., Hegd, M.S., Madras, G., 2004. Structure and photocatalytic activity of $Ti_{1-x}M_xO_{2\pm\delta}$ (M = W, V, Ce, Zr, Fe, and Cu) synthesized by solution combustion method. J. Phys. Chem. B 108, 20204–20212.

Nakano, Y., Morikawa, T., Ohwaki, T., Taga, Y., 2005. Deep-level optical spectroscopy investigation of N-doped TiO_2 films. Applied Physics Letters 86, 132104–132109.

Peng, Y.T., Chiou, S.H., Hsiao, C.H., Ouyang, C.H., Tu, C.S., 2017. Remarkably enhanced photovoltaic effects and first-principles calculations in neodymium doped $BiFeO_3$. Sci. Rep. 7, 45164.

Qi, X.H., Zhuang, Y.Y., Yuan, Y.C., Gu, W.X., 2002. Decomposition of aniline in supercritical water. J. Hazard. Mater. 90, 51–62.

Sarkar, A., Singh, A.K., Sarkar, D., Khan, G.G., Mandal, K., 2015. Three-dimensional nanoarchitecture of $BiFeO_3$ anchored TiO_2 nanotube arrays for electrochemical energy storage and solar energy conversion. ACS Sustain. Chem. Eng. 3, 2254–2263.

Taretto, K., Rau, U., 2004. Modeling extremely thin absorber solar cells for optimized design. Prog. Photovolt. Res. Appl. 12, 573–591.

Tena-Zaera, R., Katty, A., Bastide, S., Lévy-Clément, C., O'Regan, B., Muñoz-, V., 2005. Sanjosé, ZnO/CdTe/CuSCN, a promising heterostructure to act as inorganic eta-solar cell. Thin Solid Films 483, 372–377.

Wang, X., Li, Z., Xu, W., Kulkarni, S.A., Batabyal, S.K., Zhang, S., Cao, A., Wong, L.H., 2015. TiO_2 nanotube arrays based flexible perovskite solar cells with transparent carbon nanotube electrode. Nano Energy 11, 728–735.

Wang, J., Neaton, J.B., Zheng, H., Nagarajan, V., Ogale, S.B., Liu, B., Viehland, D., Vaithyanathan, V., Schlom, D.G., Waghmare, U.V., Spaldin, N.A., Rabe, K.M., Wuttig, M., Ramesh, R., 2003. Epitaxial $BiFeO_3$ multiferroic thin film heterostructures. Science 299, 1719–1722.

Wang, S., Zhang, X., Zhao, W., 2013. Flexible, transparent, and conductive film based on random networks of Ag nanowires. J. Nanomater. 2013, 3.

Wu, J., Lou, X., Wang, Y., Wang, J., 2010. Resistive hysteresis and diodelike behavior of $BiFeO_3$/ZnO heterostructure. Electrochem. Solid St. Lett. 13, G9–G12.

Wu, J., Fan, Z., Xiao, D., Zhu, J., Wang, J., 2016. Multiferroic bismuth ferrite-based materials for multifunctional applications: ceramic bulks, thin films and nanostructures. Progr. Mater. Sci. 84, 335–402.

Yanko, W.A., 1993. Analysis of 10 years of virus monitoring data from Los Angeles County treatment plants meeting California wastewater reclamation criteria. Water Environ. Res. 65, 221–226.

Zhang, S.T., Lu, M.H., Wu, D., Chen, Y.F., Ming, N.B., 2005. Larger polarization and weak ferromagnetism in quenched $BiFeO_3$ ceramics with a distorted rhombohedral crystal structure. Appl. Phys. Lett. 87, 262907.

Zhu, A., Zhao, Q., Li, X., Shi, Y., 2013. $BiFeO_3/TiO_2$ nanotube arrays composite electrode: construction, characterization, and enhanced photoelectrochemical properties. ACS Appl. Mater. Interfaces 6, 671–679.

Please cite this article in press as: Mohamed, M.M. et al., Enhanced performance of $BiFeO_3$@nitrogen doped TiO_2 core-shell structured nanocomposites: Synergistic effect towards solar cell amplification3@nitrogen doped TiO_2 core-shell –>. Arabian Journal of Chemistry (2018), https://doi.org/10.1016/j.arabjc.2018.06.013